J. Plasma Phys. (2026), *vol.* 92, E82
 doi:10.1017/S0022377826101858

Plasma wakes driven by Compton scattering: nonlinear regime and particle acceleration

Thomas Grismayer[1], Fabrizio Del Gaudio[1] and Luis O. Silva[1]

[1]GoLP/Instituto de Plasmas e Fusão Nuclear, Instituto Superior Técnico, Universidade de Lisboa, 1049-001 Lisbon, Portugal

Corresponding author: Thomas Grismayer, thomas.grismayer@tecnico.ulisboa.pt

(Received 15 January 2026 UTC; revision received 5 May 2026 UTC; accepted 18 May 2026 UTC)

We investigate plasma wake generation via Compton scattering from photon bursts in the Thomson regime, a non-ponderomotive process relevant when the photon wavelength is shorter than the interparticle distance. In this regime, electrons can reach relativistic velocities. We extend linear theory to the nonlinear regime, showing that plasma waves can reach the wave-breaking limit. Perfectly collimated drivers produce wakes propagating at the speed of light, allowing electron phase-locking (limited by driver depletion). Non-collimated drivers induce subluminal phase velocities, limiting acceleration via dephasing. Two-dimensional simulations reveal unique transverse fields compared with laser wakefields, with a DC magnetic field leading to consistent focusing. The work considers observational prospects in laboratory and astrophysical scenarios such as around highly luminous compact objects (e.g. pulsars, gamma-ray bursts) interacting with tenuous interstellar or intergalactic plasmas, where conditions favour Compton-dominated wakefield acceleration.

Key words: astrophysical plasmas, plasma simulation, plasma nonlinear phenomena

1. Introduction

Various drivers can generate plasma wakes (Tajima & Dawson 1979; Chen *et al.* 1985; Shukla *et al.* 1998). The multiplicity of potential drivers arises because different types of beams – whether collections of particles or electromagnetic fields – can interact with a plasma through an effective ponderomotive-type force. While the ponderomotive force is most commonly invoked for electromagnetic fields, the concept generalises to any field or particle ensemble with energy density $\mathcal{E}$ if the driver exerts a force $\boldsymbol{F}_{\text{pond}} \propto -\nabla\mathcal{E}$. For example, in the case of an optical laser (Tajima & Dawson 1979; Esarey *et al.* 1996; Esarey, Schroeder & Leemans 2009) or an X-ray laser (Zhang *et al.* 2016; Svedung Wettervik, Gonoskov & Marklund 2018) $\mathcal{E} \propto E^2$ with E the laser electric field. For a particle beam driver, $\mathcal{E} \propto n_b$ where n_b is the number density of an electron beam (Chen *et al.* 1985) and of a neutrino beam (Silva *et al.* 1999).

The phase velocity of the plasma wake matches that of the driving disturbance and can approach the speed of light. When the wakefield amplitude is sufficiently large, background plasma electrons may become trapped and accelerated to relativistic energies. Tajima & Dawson (1979) first identified this mechanism as a potential alternative to radio-frequency cavities in conventional accelerators and proposed that plasma wakefields could also contribute to the acceleration of cosmic rays in astrophysical environments. Although intense coherent laser pulses are unlikely to occur naturally in astrophysical scenarios, quasi-coherent electromagnetic drivers can be produced in space. Examples that have been proposed include Alfvén shocks (Chen, Tajima & Takahashi 2002), relativistic shocks in which synchrotron maser instability generates upstream precursor waves (Hoshino 2008; Kuramitsu *et al.* 2008), fast radio bursts (Petroff, Hessels & Lorimer 2019) and monster shocks (Beloborodov 2023).

Recently, Del Gaudio *et al.* (2020*a*) demonstrated that a non-ponderomotive mechanism can also drive plasma wakes. Electromagnetic drivers exert two distinct forces on plasma electrons: the familiar ponderomotive force and a second, here termed the Compton force, associated with classical radiation–reaction effects (Landau & Lifshitz 1975). For a monochromatic, collimated light beam, the Compton force is proportional to the energy density $\boldsymbol{F}_c = \sigma_T \mathcal{E}$ (Peyraud 1968; Del Gaudio *et al.* 2020*a*), where σ_T is the Thomson cross-section. The Compton force exceeds the ponderomotive force for small wavelengths or very diluted plasmas, namely $\lambda/r_0 \ll 7.7(r_e/r_0)^{1/4}$, where $r_0 = n_p^{-1/3}$ is the interparticle distance, r_e the classical electron radius, λ the wavelength and n_p the electron density.

The notion of ponderomotive force requires a quasi-classical electromagnetic field: the number of photons (of momentum $\hbar k$ with $k = 2\pi/\lambda$) in a volume k^{-3} is large compared with unity, i.e. $E/E_s \gg \sqrt{\alpha}(\hbar k/mc)^2$, where E is the electric field, $E_s = m^2c^3/e\hbar \simeq 1.3 \times 10^{18}\ \mathrm{V\,m^{-1}}$ is the Schwinger field and $\alpha = e^2/\hbar c$. One readily notes that when $\hbar k \sim mc$, the field approaches E_s; thus low-frequency fields are generally classical, while very high-frequency fields – if sufficiently weak – cannot be treated classically as discussed in Landau & Lifshitz (1982).

If the interparticle distance r_0 is large compared with k^{-1}, the dielectric description fails: photons instead Compton-scatter individual electrons in a dilute ionised gas. The electrons of the plasma are knocked by the photon burst of density n_ω at a frequency $\nu_C = (\sigma_T n_\omega c)^{-1}$. Therefore light sources composed of high-frequency photons propagating in tenuous plasma are likely to interact via Compton scattering with the plasma electrons.

Astrophysical plasmas cover a large span of densities and radiation environments, making them a fertile ground for exploring Compton-driven wakefield acceleration. While the ponderomotive force has been traditionally considered (Chen *et al.* 2002), the Compton force can dominate in tenuous plasmas or at shorter wavelengths – conditions potentially met in various astrophysical settings. From the intergalactic medium ($n_p \sim 0.01\ \mathrm{cm^{-3}}$) to pulsar magnetospheres ($n_p \sim 10^{14}\ \mathrm{cm^{-3}}$), the interparticle distance often exceeds 10 μm. Consequently, compact, energetic astrophysical objects can significantly influence their environments through interactions between radiation and plasma, resulting from the large amounts of non-thermal emission they produce. One example of conditions where the Compton force is relevant is associated with the Eddington limit; in the Thomson regime, this underlies the Eddington luminosity argument. As Blumenthal (1974) demonstrated, the classical Eddington limit, derived assuming Thomson scattering, is modified at higher photon energies due to the Klein–Nishina cross-section. This can significantly alter the radiation pressure exerted on plasma in the vicinity of compact objects. Outflows from accretion disk systems, such as active galactic nuclei and binary systems, may be launched through direct radiation pressure or the Compton rocket (Odell 1981; Phinney 1982; Henri & Pelletier 1991). Radiative interactions can also lead to drag and deceleration, depending on the specific conditions (Li, Begelman & Chiueh 1992). Madau & Thompson (2000) further explored the radiative acceleration of plasmas in the Klein–Nishina regime, relevant to compact gamma-ray sources. Their work showed that in this regime, particles can be accelerated to asymptotic Lorentz factors at infinity much more rapidly than predicted by Thomson scattering, with a reduced radiation drag due to the relativistic effects on the scattering cross-section. The analysis by Madau & Thompson (2000) also highlights the potential for 'Compton afterburn' – where random energy imparted to the plasma by gamma-rays is converted to bulk motion, supplementing the direct radiative force. Recent particle-in-cell (PIC) simulations by Faure *et al.* (2024) delve into the kinetic details of these interactions, revealing a more complex picture. They demonstrate that Compton scattering initially accelerates electrons, but the resulting charge separation also drives ions to relativistic speeds and accelerates other electrons backwards, beyond the driving photon energies. This intricate interplay, coupled with Weibel-type instabilities also shown in Martinez, Grismayer & Silva (2021) and Fermi-like scattering, leads to forward-directed suprathermal electron tails, offering a refined understanding of particle acceleration in extreme radiation environments. The variety of astrophysical sources emitting energetic radiation, such as gamma-ray bursts or pulsars, makes it plausible that Compton-dominated wakefield acceleration is a common and astrophysically relevant process. The implications for particle acceleration in these environments warrant further investigation.

In this article, we extend the one-dimensional linear theory developed in Del Gaudio *et al.* (2020*a*) to the nonlinear regime. More specifically, we investigate theoretically and numerically the wake properties and the acceleration of electrons. The analytical results are systematically compared with the PIC code OSIRIS (Fonseca *et al.* 2002), where a Compton scattering module has been implemented (Del Gaudio *et al.* 2020*b*). This paper is organised as follows. In § 2, we review the linear regime derived in a previous publication (Del Gaudio *et al.* 2020*a*), considering the cases of non-symmetric photon drivers that feature an uneven temporal profile with distinct rise and fall times, leading to asymmetric energy delivery. It allows for a more realistic modelling of complex plasma interactions driven by radiation pressure, with both practical and astrophysical relevance. Section 3 presents the one-dimensional analysis of the nonlinear regime. The acceleration of electrons in the nonlinear wake constitutes the focus of § 4. The results obtained in these sections are compared with two-dimensional simulations in § 5. Finally, in § 6 we state the conclusions and give more concrete numbers/examples about the astrophysical environments that are susceptible to match the conditions for Compton nonlinear wakes to occur.

2. Linear regime

The laser wakefield acceleration (LWFA) concept developed by Tajima & Dawson (1979) relies on a single short high-intensity laser pulse that drives a plasma wake. The wake is driven efficiently when the laser pulse length is of the order of the plasma wavelength $L \simeq \lambda_p$, where $\lambda_p = 2\pi c/\omega_p$. It is reasonable to admit that symmetric and matched coherent or laser drivers can be fine-tuned in the laboratory, but are unlikely to occur in astrophysics. In astrophysical environments, an extremely wide range of frequencies can be generated. In this section, we review and expand on the

https://doi.org/10.1017/S0022377826101858 Published online by Cambridge University Press

linear theory developed in Del Gaudio *et al.* (2020*a*), where the driver is composed of photons only interacting with electrons via Compton scattering, and extend it considering asymmetric and non-resonant drivers.

The linear theory previously developed by Del Gaudio *et al.* (2020*a*) determines the wake amplitude for a symmetric photon burst if the energy density $\mathcal{E}$ remains small compared with $\mathcal{E} \ll eE_0/\sigma_T$, where $E_0 = mc\omega_p/e$ is the classical cold wave-breaking field for a wake with phase velocity close to the speed of light (Dawson 1959). The amplitude of the wake can be computed using the electron fluid equations, continuity for the density n, momentum for the fluid velocity βc and Poisson's equation for the longitudinal field E_x. The averaged fluid force exerted by the photon burst is $\sigma_T\mathcal{E}$. The set of equations reads

$$\frac{\partial n}{\partial t} = -c\frac{\partial}{\partial x}(n\beta), \tag{2.1}$$

$$mc\frac{\mathrm{d}\beta}{\mathrm{d}t} = -eE_x + \sigma_T\mathcal{E}, \tag{2.2}$$

$$\frac{\partial E_x}{\partial x} = 4\pi e(n_p - n), \tag{2.3}$$

where n_p is the plasma density. The ions are assumed to be immobile. The linearised version of this set of equations is

$$\frac{\partial n_1}{\partial t} = -cn_p\frac{\partial \beta_1}{\partial x}, \tag{2.4}$$

$$mc\frac{\partial \beta_1}{\partial t} = -eE_x + \sigma_T\mathcal{E}, \tag{2.5}$$

$$\frac{\partial E_x}{\partial x} = -4\pi e n_1, \tag{2.6}$$

where the electron density is written as $n = n_p + n_1$. The plasma is considered to be initially at rest, implying $\beta = \beta_1$. The change of variables $\tau = \omega_p t$, $\xi = k_p(x - ct) = k_p x - \tau$, $k_p = \omega_p/c$ leads to

$$\frac{\partial}{\partial \tau}\left(\frac{n_1}{n_p}\right) = \frac{\partial}{\partial \xi}\left(\frac{n_1}{n_p} - \beta_1\right), \tag{2.7}$$

$$\frac{\partial \beta_1}{\partial \tau} = \frac{\partial \beta_1}{\partial \xi} - \frac{E_x}{E_0} + \frac{\sigma_T\mathcal{E}}{mc\omega_p}, \tag{2.8}$$

$$\frac{\partial}{\partial \xi}\left(\frac{E_x}{E_0}\right) = -\frac{n_1}{n_p}. \tag{2.9}$$

The quasi-static approximation, commonly used in the theory of LWFA (Sprangle, Esarey & Ting 1990), neglects $\partial/\partial\tau$ in the electron fluid equations, which is valid when the driver evolution time is long compared with the transit time of the plasma through the driver, i.e. $\omega \gg \omega_p$ for a laser of frequency ω. In the case of an uncoherent photon driver (made of photons of frequency ω and density n_ω), the typical evolution time of the burst envelope is $t_\omega = \nu_\omega^{-1} = (\sigma_T n_p c)^{-1}$. For a driver with arbitrary duration τ_d, we have $t_\omega \gg \tau_d$, which is equivalent to $n_p r_e^3 \ll (\omega_p \tau_d)^{-2}$, a criterion that is generally satisfied for all astrophysical and laboratory plasmas. The equation for the electrostatic field is now

$$\left(\frac{\partial^2}{\partial \xi^2} + 1\right) E_x = \sigma_T \mathcal{E}. \tag{2.10}$$

The solution for the longitudinal field is given by the convolution of the source term with the Green function of the harmonic operator:

$$E_x = \sigma_T \mathcal{E}_0 \int_0^{-k_p L} \sin(\xi - s) f(s) \mathrm{d}s, \tag{2.11}$$

where $\mathcal{E}(s) = \mathcal{E}_0 f(s)$, f being the bounded shape function of the driver, and $L = c\tau_d$ is the length of the driver. Integration by parts of the integral $I = \int_0^{-k_p L} \mathrm{d}s \sin(\xi - s) f(s)$ yields

$$I = \cos(\xi - s) f(s)\Big|_0^{-k_p L} + \int_0^{-k_p L} \mathrm{d}s \cos(\xi - s) \frac{\partial f}{\partial s}, \tag{2.12}$$

where $f(s)\Big|_0^{-k_p L} = 0$ is imposed since f is bounded. To understand the influence of the shape of the driver on the amplitude of the wake, we consider a driver of triangular shape characterised by a rise time RL/c and a fall length $(1 - R)L/c$, where R is the rise time normalised to L/c. With the choice of f, the integral given by (2.12) has an exact solution:

$$I = \frac{1}{k_p} \mathcal{A} \cos(\xi + \theta), \tag{2.13}$$

$$\mathcal{A} = \sqrt{a^2 + b^2}, \tag{2.14}$$

$$\theta = \arctan(b/a), \tag{2.15}$$

where

$$a = \frac{\cos(Rk_p L) - 1}{Rk_p L} + \frac{\cos(k_p L) - \cos(Rk_p L)}{(1 - R)k_p L}, \tag{2.16}$$

$$b = \frac{\sin(Rk_p L)}{Rk_p L} + \frac{\sin(k_p L) - \sin(Rk_p L)}{(1 - R)k_p L}. \tag{2.17}$$

From (2.16) and (2.17), we observe that whenever $Rk_p L \lesssim 1$ or $(1 - R)k_p L \lesssim 1$, the wake amplitude $\mathcal{A} \sim 1$ and does not diminish with respect to $k_p L$, even for non-resonant long drivers $k_p L \gg 1$. If instead $Rk_p L \gg 1$ or $(1 - R)k_p L \gg 1$ then $\mathcal{A} \propto 1/k_p L$.

These scalings are shown in figure 1 where the amplitude of the function $\mathcal{A}$ is plotted as a function of $k_p L$ for two cases: $Rk_p L \ll 1$ and $R = 0.5$. We have also verified these scalings with one-dimensional PIC simulations. The burst is composed of photons of energy $\hbar\omega = 0.001\, mc^2$ with $\mathcal{E}_0 = 0.01 eE_0/\sigma_T$ propagating in

https://doi.org/10.1017/S0022377826101858 Published online by Cambridge University Press

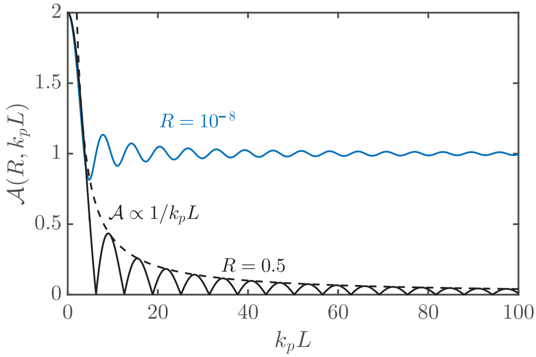

FIGURE 1. Amplitude of the function $\mathcal{A}$ as a function of k_pL given by (2.14) plotted in solid line for $R = 10^{-8}$ in blue and for $R = 0.5$ in black. For a long driver $k_pL \gg 1$, if $Rk_pL \lesssim 1$, the wake amplitude does not decrease. For a symmetric driver $R = 0.5$, the wake amplitude falls as $\mathcal{A} \propto 1/k_pL$, shown in dashed line.

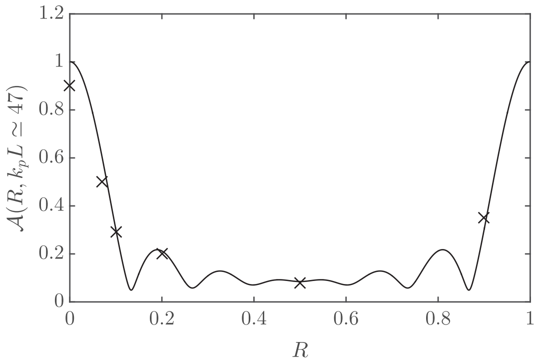

FIGURE 2. Amplitude of the function $\mathcal{A}$ as a function of R given by (2.14) plotted in solid line for $k_pL \simeq 47$. One-dimensional PIC simulation results are displayed with crosses, showing excellent agreement with the theoretical prediction for the maximum amplitude of the wake.

a cold plasma of uniform density $n_p = 1\ \mathrm{cm}^{-3}$. The simulations are performed with a moving window $100\, d_e$ long ($d_e = k_p^{-1}$), with $\Delta x = 0.01 k_p^{-1}$, and $\Delta t = 0.0099\, \omega_p^{-1}$. The number of particles in each cell is 100, and the burst is made of photons of energy $\hbar\omega = 0.001\, mc^2$ with $\mathcal{E}_0 = 0.01 eE_0/\sigma_T$. Figure 2 shows the amplitude of the function $\mathcal{A}$ as a function of R, given by (2.14) for $k_pL \simeq 47$ obtained from (2.14), in solid line, and from simulations, denoted by crosses, demonstrating the excellent agreement between theory and simulations.

3. Nonlinear regime

We consider now the case of a photon burst with an energy density sufficiently high to push electrons into relativistic motion. The nonlinear regime of plasma wakes, which has been extensively studied for laser drivers by Sprangle *et al.* (1990) and Esarey *et al.* (1996), is reached when the plasma electric field approaches the wave-breaking limit. In our case, the photon energy density must be capable of generating a wake amplitude E_0 – the photon energy density being of the order

https://doi.org/10.1017/S0022377826101858 Published online by Cambridge University Press

of $\mathcal{E}_0 \sim eE_0/\sigma_T$. Using the definition of E_0, it corresponds to a photon energy density of

$$\mathcal{E}_0 \sim 10^{12}\sqrt{n[\mathrm{cm}^{-3}]}\,\mathrm{erg\,cm}^{-3} \tag{3.1}$$

The amplitude of the Langmuir wake driven by the burst can be derived by solving the following system of equations:

$$\begin{aligned}
\frac{\partial n}{\partial t} &= -c\frac{\partial}{\partial x}(n\beta),\\
mc\frac{\mathrm{d}\gamma\beta}{\mathrm{d}t} &= -eE_x + \sigma_T\mathcal{E}\frac{1-\beta}{1+\beta},\\
\frac{\partial E_x}{\partial x} &= 4\pi e(n_p - n),
\end{aligned} \tag{3.2}$$

where the momentum equation includes the relativistic fluid version of the Compton force, in the limit $\hbar\omega \ll mc^2$. A version of the relativistic Compton force valid for all photon energies can be found in Blumenthal (1974) and Faure *et al.* (2024). Rewriting (3.2) as a function of τ and ξ, and using the quasi-static approximation, we obtain

$$\begin{aligned}
\frac{\partial}{\partial \xi}(n(1-\beta)) &= 0,\\
\frac{\partial}{\partial \xi}(\gamma(\beta-1)) &= \frac{E_x}{E_0} - \frac{\sigma_T\mathcal{E}}{eE_0}\frac{1-\beta}{1+\beta},\\
\frac{\partial}{\partial \xi}\left(\frac{E_x}{E_0}\right) &= 1 - \frac{n}{n_p}.
\end{aligned} \tag{3.3}$$

The continuity equation implies $n(1-\beta) = n_p$, and Poisson's equation in (3.3) can thus be rewritten as $\partial_\xi(E_x/E_0) = \beta/(\beta-1)$. Deriving the momentum equation with respect to ξ and substituting into Poisson's equation, we arrive at a second-order equation for β:

$$\frac{\partial^2}{\partial \xi^2}(\gamma(\beta-1)) + \frac{\beta}{1-\beta} + \frac{\partial}{\partial \xi}\left(\frac{\sigma_T\mathcal{E}}{eE_0}\frac{1-\beta}{1+\beta}\right) = 0. \tag{3.4}$$

In the limit $\beta \ll 1$, the linear theory is recovered. Poisson's equation becomes $\partial_\xi(E_x/E_0) = -\beta$, and the momentum equation (3.3) becomes $\partial_{\xi^2}\beta + \beta + \partial_\xi(\sigma_T\mathcal{E}/eE_0) = 0$.

The nonlinear theory for the laser wakefield, reviewed by Esarey *et al.* (1996), determines the maximum amplitude of a driven plasma wave. Behind the driver, where $\mathcal{E} = 0$, the conditions $\partial_\xi(E_x/E_0) = \beta/(\beta-1)$ and $\partial_\xi[\gamma(\beta-1)] = (E_x/E_0)$ hold. Simple algebra shows that these equations are equivalent to $\partial_\xi(E_x/E_0)^2/2 + \partial_\xi\gamma = 0$, which can be interpreted as an energy conservation law:

$$\frac{1}{2}\frac{E_x^2}{E_0^2} + \gamma = \gamma_m, \tag{3.5}$$

where the E_x^2 term is the energy density stored in the field, γ is the normalised energy of the electron fluid and γ_m is a constant given by the maximum Lorentz factor of the electron fluid, when $E_x = 0$ behind the driver. The field amplitude is maximum when the electron fluid is at rest, $\gamma = 1$, leading to

$$E_{\max} = E_0\sqrt{2(\gamma_m - 1)}. \tag{3.6}$$

This is the expression of the cold relativistic wave-breaking limit (Akhiezer & Polovin 1956; Esarey *et al.* 1996) when $\gamma_m = \gamma_\phi$, where γ_ϕ is the relativistic factor associated with the phase velocity of the plasma wave. As already demonstrated in the previous work by Del Gaudio *et al.* (2020*a*), and further discussed in this article, a collimated photon driver propagates at the vacuum speed of light inside the plasma, which implies $\gamma_\phi \to \infty$. Nonetheless, the value of $E_{\max}$ and γ_m must be finite for a given finite photon energy density $\mathcal{E}_0$.

The amplitude of the electric field is determined by the Compton force. Incorporating relativistic fluid corrections introduces a velocity dependence into the driver force, necessitating an estimate of the factor $(1-\beta)/(1+\beta)$. When $\sigma_T\mathcal{E}_0 \gg eE_0$, we may expect β to approach unity in the driver region. The Poisson equation becomes $\partial_\xi(E_x/E_0) \simeq 1/(\beta - 1)$, and we can then estimate the amplitude of the resulting wake by equating the field and the Compton force:

$$\frac{E_x}{E_0} \simeq \frac{\sigma_T\mathcal{E}}{eE_0}\frac{E_0}{2\partial_\xi E_x}, \tag{3.7}$$

which gives

$$\frac{E_{\max}^2}{E_0^2} \simeq \int_0^\pi \frac{\sigma_T\mathcal{E}}{eE_0}\,\mathrm{d}\xi. \tag{3.8}$$

In the case of a resonant driver with shape $\mathcal{E} = \mathcal{E}_0\sin^2(\xi/2)$, we obtain that

$$\frac{E_{\max}}{E_0} \simeq \sqrt{\pi\frac{\sigma_T\mathcal{E}_0}{eE_0}}. \tag{3.9}$$

This indicates that, unlike in the linear regime, the wake amplitude scales as the square root of the photon energy density. Using (3.6), we deduce that

$$\gamma_m \simeq \frac{\sigma_T\mathcal{E}_0}{eE_0} = \frac{\nu_c}{\omega_p}\frac{\hbar\omega}{mc^2}. \tag{3.10}$$

Figure 3 shows the amplitude of the wakefield E_x/E_0 (in black lines) and the fluid momentum of the plasma electrons $\gamma\beta$ (in blue lines) for a peak energy density $\mathcal{E}_0 = eE_0/\sigma_T$. The maximum momentum of the electron fluid over the plasma oscillations is $\gamma\beta \simeq 1$, which implies a maximum Lorentz factor of $\gamma_{\max} \simeq 1.4$. We compared the numerical solution of (3.4) and the predictions of (3.6) and (3.10) with one-dimensional PIC simulations in the nonlinear regime $\sigma_T\mathcal{E}_0 \sim eE_0$. The simulations are performed with a moving window in a box $24k_p^{-1}$ long, filled with a cold plasma of density $n_p = 1\ \mathrm{cm}^{-3}$. The spatial resolution is chosen to be $\Delta x = 0.001k_p^{-1}$, the time step $\Delta t = 0.00099\,\omega_p^{-1}$ and the number of particles per cell is 30. The burst is composed of photons of energy $\hbar\omega = 0.01\,mc^2$, with a Gaussian shape $\mathcal{E} = \mathcal{E}_0\cos^2(\pi\xi/L)$, $\xi \in [-L, 0]$, and is resonant $L = \lambda_p$ (the duration of the burst is $\tau_p = L/c \simeq 0.1$ ms) to maximise the amplitude of the electric field.

https://doi.org/10.1017/S0022377826101858 Published online by Cambridge University Press

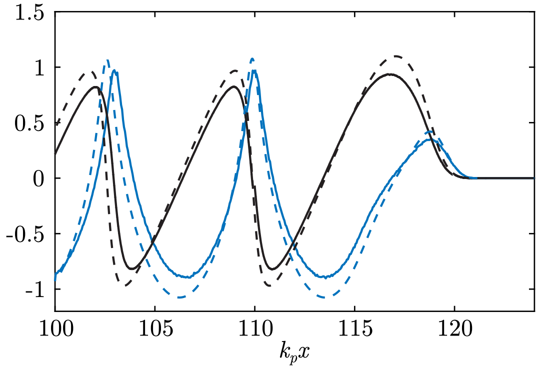

FIGURE 3. Amplitude of the wakefield (black) and normalised fluid momentum of the plasma electrons (blue) for a resonant driver with energy density of $\mathcal{E}_0 = eE_0/\sigma_T$. The simulation results are shown as a solid line, and the theory, the solution of (3.4), as a dashed line.

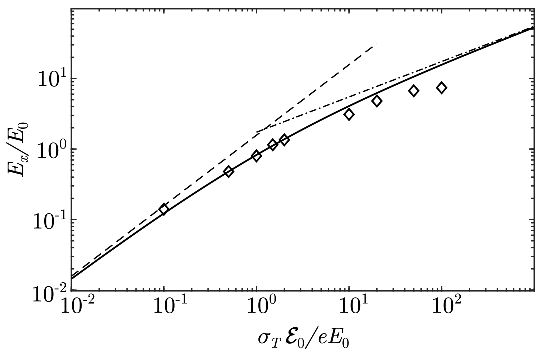

FIGURE 4. Amplitude of the wakefield as a function of the driver energy density. Simulations are denoted with ($\diamond$). The numerical solution of (3.4) is shown as a solid line, (3.6) with γ_m obtained from (3.10) as a dot-dashed line and linear theory as a dashed line.

Figure 4 illustrates the amplitude of the wakefield as a function of the peak energy density for a resonant driver. As expected, the results deviate from linear theory, represented by the dashed line. The nonlinear theory, described by (3.4) and shown with a solid line, aligns well with PIC simulation results, indicated by ($\diamond$). Additionally, the dot-dashed line corresponds to (3.6) with $\gamma_{\max}$ obtained from (3.10), and it agrees with the numerical solution of (3.4). At higher energy densities, the theory increasingly diverges from simulation outcomes, which indicate that the kinetic effects – absent in cold-fluid models – become significant. The simulations seem to indicate that a portion of the driver energy is diverted into plasma thermal energy rather than solely contributing to electron fluid motion. Figure 5 depicts the wake's wavelength as a function of the peak energy density $\mathcal{E}_0 = eE_0/\sigma_T$. The nonlinear theory (3.4) (solid line) agrees with PIC simulations (denoted by ($\diamond$)). As electron velocities approach relativistic speeds, plasma oscillations decrease in frequency ($\omega_p \rightarrow \omega_p/\sqrt{\gamma_m}$) and experience an increase in wavelength ($\lambda_p \rightarrow \sqrt{\gamma_m}\lambda_p$), due to the relativistic increase in electron mass.

https://doi.org/10.1017/S0022377826101858 Published online by Cambridge University Press

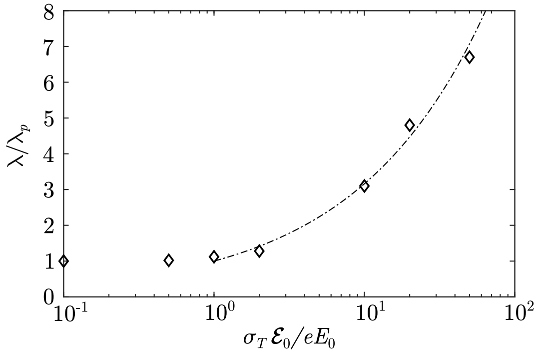

FIGURE 5. Wavelength of the wake as a function of the driver energy density. Simulations are denoted with ($\diamond$). The solid line is $\sqrt{\gamma_m}\lambda_p$ with γ_m given by (3.10).

4. Acceleration of leptons

Plasma wakes with phase velocities approaching the speed of light were first demonstrated experimentally by Clayton *et al.* (1985) and shown to be effective and robust structures for accelerating electrons to ultra-relativistic energies by three research groups in 2004 (Faure *et al.* 2004; Geddes *et al.* 2004; Mangles *et al.* 2004) and later for positrons by Corde *et al.* (2015).

Accordingly, a natural application of our work – regarding plasma wakes driven by photon bursts via the Compton force – is the acceleration of electrons. At first glance, one might assume that insights from LWFA (Esarey *et al.* 1996; Esarey *et al.* 2009) would suffice to allow conclusions about leptons acceleration through Compton scattering. However, there are notable differences that merit emphasis. In this section, we review the primary physical mechanisms known to limit electron acceleration – namely wake phase velocity, dephasing, driver diffraction and driver depletion. For each mechanism, we provide a quantitative analysis and compare the findings with the established results in the laser-driven wakefield context.

4.1. *Collimated photon driver*

Previous work by Del Gaudio *et al.* (2020*a*) demonstrated that a radiation burst consisting of photons with wavelengths much shorter than the interparticle distance of plasma electrons does not experience light dispersion, as the concept of a dielectric medium does not apply here. In fact, these photons do not perceive the plasma as a macroscopic, collective medium but rather as a rarefied gas. They propagate at the speed of light between successive Compton scattering events, which gradually deplete the photon population within the burst. Consequently, a perfectly collimated photon burst travels at the speed of light through the plasma for a time $t \ll \nu_\omega^{-1}$. This behaviour is fundamentally different from the propagation of a typical laser pulse, which travels at its group velocity. In an unmagnetised plasma, electromagnetic wave dispersion limits the Lorentz factor associated with the wave group velocity to $\gamma_g = (1-\beta_g^2)^{-1/2} = \omega/\omega_p$, where $\beta_g c$ is the group velocity and ω is the wave frequency. It is well established that an electrostatic wakefield excited by a laser driver exhibits a phase velocity $\beta_\phi = \beta_g$. The phase velocity of the wake critically determines the maximum energy gain that an accelerated charged particle can achieve. During acceleration, a particle can reach velocities exceeding the wake phase velocity and consequently outrun the plasma wave. When this occurs, acceleration ceases, and the maximum attainable particle energy is limited by dephasing. The phenomena of trapping, acceleration and dephasing of charged particles have been extensively studied in one dimension (Esarey & Pilloff 1995; Esarey *et al.* 1996; Esarey *et al.* 2009). In both linear and nonlinear regimes, the maximum Lorentz factor of an accelerated charge scales as $\gamma_{\max} \propto \gamma_\phi^2$.

To examine the acceleration of electrons within the wake generated by a collimated photon burst, we initially neglect the depletion of the driver. The primary objective is to analyse the trapping conditions when the phase velocity equals the speed of light. In this scenario, an electron captured at the front of the accelerating region of the plasma wave cannot overtake the wave front at any subsequent time. Consequently, the electron will continuously accumulate a phase difference relative to the wake and eventually slip backwards, never outrunning the plasma wave. For simplicity, in the following model, the wake is assumed to have a square-shaped profile. Formally, the wakefield can be expressed as

$$E(x,t) = E_x \operatorname{sign}\left[\sin(k_p(x-ct))\right]. \tag{4.1}$$

A more rigorous calculation can be carried out with a sine function, but it turns out to be cumbersome without changing the final result. The accelerating field E_x is thus constant on half a wavelength, and as long as the electron does not slip back. The motion $X(T) = e|E_x|x(t)/mc^2$ of an electron injected at the front X_f at time $T = e|E_x|t/mc = 0$ with initial momentum $p_0 = mc\sqrt{\gamma_0^2 - 1}$ can be derived analytically. The momentum evolves as $p = e|E_x|t + p_0$ and the energy as $\gamma = \sqrt{1 + (T + p_0/mc)^2}$. Integrating the equation of motion leads to

$$\frac{\mathrm{d}X}{\mathrm{d}T} = \frac{T + p_0/mc}{\sqrt{1 + (T + p_0/mc)^2}}, \tag{4.2}$$

$$X = \sqrt{1 + (T + p_0/mc)^2} - \gamma_0. \tag{4.3}$$

The distance of the electron to the front of the acceleration region, which moves at the speed of light $X_f(T) = T$, is $\Delta X(T) = X_f(T) - X(T)$, or

$$\Delta X = T + \gamma_0 - \sqrt{1 + (T + p_0/mc)^2}. \tag{4.4}$$

The acceleration persists until the phase-slip distance $l_\phi = mc^2 \Delta X/e|E_x|$ exceeds the length of the acceleration region, which we take to be half the plasma wavelength, i.e. $l_\phi > \lambda_p/2$. Furthermore, over sufficiently long times, the distance ΔX becomes effectively time-independent:

$$\Delta X^\infty = \lim_{T\to\infty} \Delta X = \gamma_0 - p_0/mc. \tag{4.5}$$

This situation echoes the longitudinal invariance of an electron in a plane electromagnetic wave. If the asymptotic phase-slip distance $l_\phi^\infty = mc^2 \Delta X^\infty/e|E_x|$ remains shorter than the length of the acceleration region ($\lambda_p/2$), the electron will become phase-locked with the wake. This implies that the worldline of the electron always remains outside the light cone of the rear boundary of the accelerating zone, as illustrated in figure 6. The phase-locking condition, expressed in terms of the electric field of the wave, is given by

$$\frac{|E_x|}{E_0} \gtrsim \frac{1}{\pi}\left(\gamma_0 - \frac{p_0}{mc}\right). \tag{4.6}$$

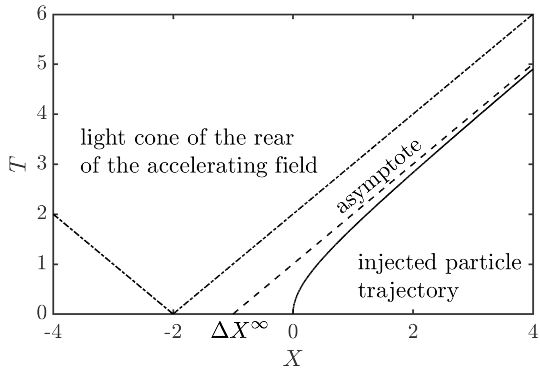

FIGURE 6. Example of phase-locking condition. The particle trajectory (solid line) converges to its asymptotic (dashed line) $T = X + \Delta X^{\infty}$ and will never enter the light cone of the rear of the accelerating zone (dot-dashed), set at $X = -2$ initially.

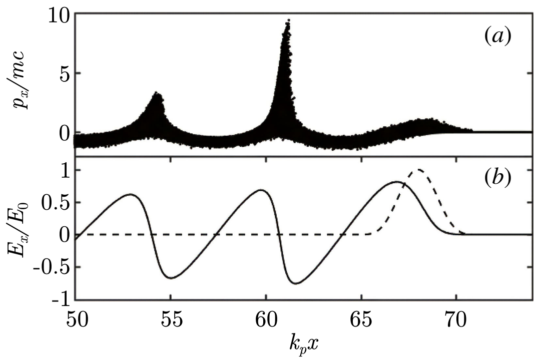

FIGURE 7. One-dimensional simulation of electron acceleration in a wake driven by Compton scattering. A resonant burst of energy density $\mathcal{E} = eE_0/\sigma_T$ with 50 keV photons propagates in a plasma of density $n_p = 10^{18}\ \mathrm{cm}^{-3}$. ($a$) Longitudinal momentum of the electrons p_x. (b) Longitudinal wakefield E_x (solid line) and photon driver density in arbitrary units (dashed line).

For an electron initially at rest, it reads $|E_x| \gtrsim E_0/\pi$, which is rather constraining since the field should be of the order of the cold wave-breaking limit. The condition for trapping and phase locking is considerably lower for an ultra-relativistic injected electron $\gamma_0 \gg 1$, which amounts to $E_x > E_0/(2\pi\gamma_0)$. We point out that these results are only valid for the special case $\beta_\phi = 1$. For LWFA, $\beta_\phi = \beta_g < 1$, although β_g approaches unity for low plasma density or high frequency.

We validated the electron acceleration process through PIC simulations. In these simulations, the photon burst consists of 5×10^5 macro-photons, each with an energy of 50 keV, corresponding to the normalised amplitude $\mathcal{E}_0 = eE_0/\sigma_T$. The photons propagate along the x axis and interact with an initially cold plasma of density $n_p = 10^{18}\ \mathrm{cm}^{-3}$, represented by 32 macro-electrons per simulation cell. The simulations employ a moving window of length $24k_p^{-1}$, discretised into 24 000 grid cells. The time step Δt is set to $(1 - 10^{-6})\Delta x$ to minimise the numerical dispersion of the wake, thus ensuring Courant stability. Figure 7 displays the early stage of the acceleration process after a propagation distance of $15k_p^{-1}$. Figure 7(a) shows the longitudinal

https://doi.org/10.1017/S0022377826101858 Published online by Cambridge University Press

momentum distribution of electrons, revealing characteristic signatures of trapping and acceleration near the rear of the wake. Figure 7(*b*) depicts the corresponding electrostatic field: the solid line represents the field behind the driver, shown by the dashed line. In this simulation, the measured wakefield amplitude is $E_{\max} = 0.74E_0$, which aligns well with (3.4) that predicts $E_{\max} \simeq 0.78E_0$. Since the cold wave-breaking field is nearly reached, electrons can be trapped in the wake from rest, consistent with (4.6). A detailed examination of the simulation data indicates that the trapped particles do not precisely occupy the region of maximum field. Instead, the maximum accelerating field experienced by the trapped electrons is $E_{acc} = 0.61E_0$. Additionally, simulations incorporating a 10 % energy spread in the photon driver were conducted; these show no significant impact on wake excitation or electron acceleration, as expected based on Del Gaudio *et al.* (2020*a*).

The prospect of electrons remaining phase-locked indefinitely implies that dephasing may not constrain the maximum energy in a Compton wakefield accelerator, unlike in laser- or plasma-based schemes. However, this result is valid only for an idealised, non-evolving driver. For any realistic driver, multiple factors contribute to limiting the maximum achievable energy of an accelerated electron. In general, the maximum Lorentz factor can be expressed as

$$\gamma_{\max} \simeq \frac{E_x}{E_0}\frac{l_a}{d_e}, \tag{4.7}$$

where l_a is the length over which the electron can be accelerated. In the following sections, we examine the effects of driver depletion and diffraction.

4.2. *Driver depletion*

As the burst generates the plasma wake, the finite energy content of the driver is gradually depleted, which in turn impacts the sustainability of the plasma wake. In LWFA, it is well established that the laser pulse depletes as it drives the plasma wave. The pump depletion length L_{pd} can be estimated by equating the initial laser energy to the energy transferred to the wakefield as shown by Esarey *et al.* (1996, 2009) and Shadwick, Schroeder & Esarey (2009), which leads to $L_{dp} \simeq (\lambda_p^3/\lambda) f(a_0)$ with $f(a_0) = 2/a_0^2$ if $a_0 \ll 1$ or $f(a_0) = \sqrt{2}/\pi a_0$ if $a_0 \gg 1$.

The photons that transfer momentum to the plasma electrons are deflected and eventually exit the driver. Similar to the laser case, significant electron acceleration can only occur within the characteristic depletion length of the driver. This length corresponds to the mean free path of a photon, given by $l_{dp} = (\sigma_T n_p)^{-1}$. Consequently, the maximum Lorentz factor attainable is

$$\gamma_{\max} \sim \frac{E_x}{E_0}\frac{l_{dp}}{d_e}. \tag{4.8}$$

For a dense plasma of density $n_p = 10^{18}\,\mathrm{cm}^{-3}$ the electron inertial length is $d_e \simeq 5.3\,\mu\mathrm{m}$ and the depletion length would be $l_{dp} \simeq 15.4\,\mathrm{km}$. Conducting kinetic simulations across this vast scale separation is computationally unfeasible. To circumvent this limitation, we artificially increase the scattering cross-section by a factor $M = 10^6$, such that $\sigma_T \rightarrow M\sigma_T$. This numerical rescaling enables us to observe the saturation of acceleration within a feasible simulation timeframe. Figure 8 illustrates the saturation of the maximum Lorentz factor $\gamma_{\max}$ measured after a propagation distance of approximately $l \simeq 2l_{dp}/d_e$. The acceleration ceases when the electric field

https://doi.org/10.1017/S0022377826101858 Published online by Cambridge University Press

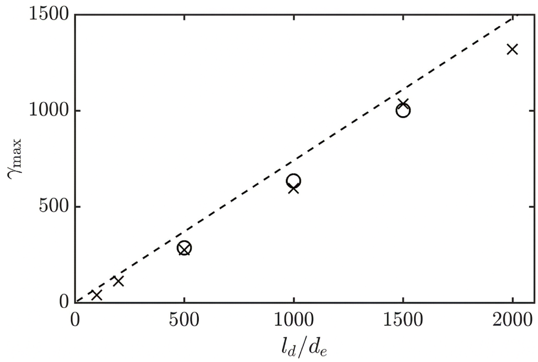

FIGURE 8. Maximum Lorentz factor γ_{max} as a function of the driver depletion length l_d. Theory (dashed line) refers to the maximum field $E = 0.74E_0$. Simulations (crosses) with parameters: $\mathcal{E} = eE_0/\sigma_T$, 50 keV photons and $n_p = 10^{18}\ \mathrm{cm}^{-3}$. The depletion length has been artificially reduced (with a factor $M = 10^6$) to observe the saturation of the acceleration. The introduction of a 10 % energy spread in the photon driver (circles) shows no influence on the acceleration process.

diminishes to a level where the accelerated particles can no longer stay phase-locked with the wake. Notably, the simulation results agree with our estimate, derived from (4.8), within a relative error of about 10 %.

4.3. *Non-collimated driver*

A spread in the transverse component of the photon distribution is another effect that limits the acceleration of electrons. If the driver is not collimated, its ensemble velocity is lower than the velocity of light and corresponds to the average velocity along the propagation direction $\hat{\boldsymbol{k}}_0$. Assuming a Gaussian spread σ in the transverse direction, the photon distribution function can be written as

$$\mathcal{N}(\boldsymbol{k}) = \frac{1}{2\pi\sigma^2} \exp\left(-\frac{\boldsymbol{k}_\perp^2}{2\sigma^2}\right)\delta(\boldsymbol{k}_\parallel - \boldsymbol{k}_0). \tag{4.9}$$

We define

$$\begin{aligned} \langle \tan\alpha \rangle &= \int \mathrm{d}\boldsymbol{k} \frac{k_\perp}{k_\parallel}\mathcal{N}(\boldsymbol{k}) \\ &= \sqrt{\frac{\pi}{2}}\frac{\sigma}{k_0}. \end{aligned} \tag{4.10}$$

For $\sigma/k_0 \ll 1$, the average angle is $\langle\alpha\rangle \simeq \sqrt{\pi/2}(\sigma/k_0)$. The ensemble velocity along $\boldsymbol{k}_0$ is related to α via $\langle\beta_e\rangle = \langle\cos\alpha\rangle$ which gives for $\alpha \ll 1$

$$\langle\beta_e\rangle \simeq 1 - \frac{1}{2}\langle\alpha^2\rangle = 1 - \frac{2}{\pi}\langle\alpha\rangle^2. \tag{4.11}$$

The simulations presented in this section are performed with a moving window $36k_p^{-1}$ long, with resolution $\Delta x = 0.001\ d_e$ and time step $\Delta t = 0.00099\ \omega_p^{-1}$. The number of particles per cell is 30. The driver is composed of photons of energy $\hbar\omega = 0.01\ mc^2$

https://doi.org/10.1017/S0022377826101858 Published online by Cambridge University Press

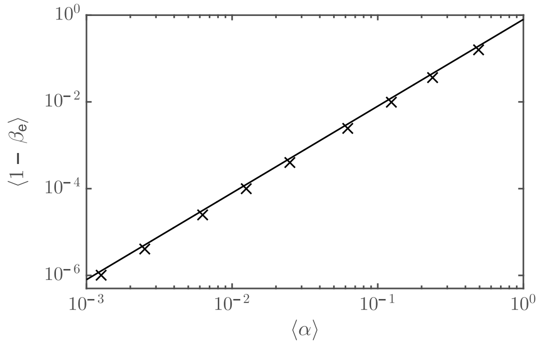

FIGURE 9. Ensemble longitudinal velocity of the photon burst as a function of the divergence angle $\langle\alpha\rangle$. Equation (4.11) is shown as a solid line and simulations as crosses.

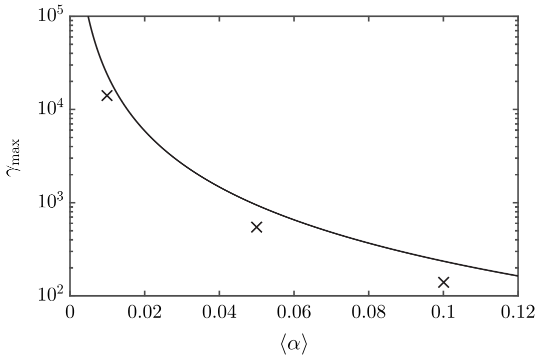

FIGURE 10. Maximum Lorentz factor as a function of $\langle\alpha\rangle$ given by dephasing. Simulations are shown as crosses and (4.7) as a solid line, where $l_a = l_d$ and $E_x = 0.61E_0$ corresponding to a resonant driver energy density of $\mathcal{E}_0 = eE_0/\sigma_T$.

with $\mathcal{E}_0 = eE_0/\sigma_T$ and the distribution is initialised according to (4.9). The reference plasma density is always taken to be $n_p = 1\ \text{cm}^{-3}$.

Figure 9 illustrates the ensemble longitudinal velocity of the photon burst, which aligns with the predictions of (4.11). As the driver's energy is transferred to the plasma to excite the wake, the phase velocity of the wake β_ϕ is inherently equal to the ensemble velocity of the photon burst, i.e. $\beta_\phi = \beta_e$. In this scenario, electron acceleration would be limited by dephasing, analogous to the case in LWFA. The dephasing length for linear and mildly nonlinear wakes is approximately $l_d \simeq \gamma_\phi^2\lambda_p$ (Tajima & Dawson 1979; Esarey & Pilloff 1995), where γ_ϕ is the Lorentz factor associated with the wake phase velocity. Using (4.11) leads to $\gamma_\phi^2 = (\pi/4)/\langle\alpha\rangle^2$, which gives

$$l_d \simeq \frac{\pi}{4}\frac{\lambda_p}{\langle\alpha\rangle^2}. \tag{4.12}$$

Figure 10 shows the maximum Lorentz factor as a function of dephasing, with simulations as crosses and a solid line representing the theoretical model from (4.7) and (4.12).

https://doi.org/10.1017/S0022377826101858 Published online by Cambridge University Press

We emphasise that dephasing occurs systematically in laser plasma accelerators, even with non-evolving pulses. In contrast, for Compton-driven wakes, dephasing effects are only significant when the driver deviates from ideal conditions.

5. Two-dimensional effects

The one-dimensional theory and simulations of Compton wakes assume that the photon driver has an arbitrarily large transverse extent. However, the longitudinal properties of these wakes should remain valid as long as the driver's width exceeds its length. It is well known from laser wakefield theory that finite beam width introduces focusing fields in the wake, and in the limit of the blowout regime, the wake adopts a bubble-shaped structure as first observed by Pukhov & Meyer-ter Vehn (2002), and further investigated in depth theoretically (Lu *et al.* 2006) and numerically (Lu *et al.* 2007). This regime is considered optimal for electron acceleration but requires precise tuning of the laser pulse profile with the plasma density. Consequently, such conditions are unlikely to be readily achievable outside controlled laboratory settings. A similar reasoning could be applied to a photon driver. Nonetheless, for the sake of curiosity, it is legitimate to question whether the properties of two-dimensional wakes generated by laser pulses differ from those produced by photon drivers. To explore this, we numerically investigate two-dimensional wake structures generated by various photon drivers, varying both the amplitude and the transverse width, in both the linear and nonlinear regimes. For simplicity, we restrict our study to collimated photon drivers. In the case of laser-driven plasma wakes, the transverse fields can generally be estimated from the longitudinal fields using the Panofsky–Wenzel theorem (Panofsky & Wenzel 1956), assuming electrons are primarily accelerated along the longitudinal direction and are sufficiently relativistic. In two-dimensional Cartesian geometry, and in the limit where $\beta_x \to 1$, the theorem states that $\partial_\xi (E_y - B_z) \simeq \partial_y E_x$. As we will see, the theorem does not hold for a Compton-driven wake.

5.1. *Two-dimensional linear regime*

The two-dimensional simulations are performed in a moving window $50d_e \times 30d_e$ long and wide, respectively, with resolution $\Delta x = 0.01 d_e$ and time step $\Delta t = 0.007\omega_p^{-1}$. The number of particles in each cell is 256. The driver is always resonant and composed of photons of energy in the range $\hbar\omega = (0.001-0.01)mc^2$, and the reference plasma density is $n_p = 1\ \mathrm{cm}^{-3}$. All the figures show: (*a*) the plasma density, (*b*) the longitudinal electric field and (*c*) the total transverse field.

The simulations with an infinite width are performed with periodic boundary conditions. Figure 11 corresponds to a driver in the linear regime $\mathcal{E}_0 = 0.01\, eE_0/\sigma_T$. In this regime, the amplitude of the wake is $E_x = (\pi/2)\sigma_T \mathcal{E}_0/e$, which gives $E_x/E_0 = (\pi/2) \times 10^{-2}$ for the parameter of the simulation, which is in agreement with figure 11(*b*). The transverse fields shown in figure 11(*c*) vanish as expected in the linear regime for an infinitely wide driver since $\partial_y E_x = 0$.

For a round photon driver that possesses in both longitudinal and transverse directions an identical density profile:

$$\mathcal{E}(x, y, t) = \mathcal{E}_0 \sin^2(\xi/2) \cos^2(\pi y/L_y), \tag{5.1}$$

with $\xi = k_p(x - ct) \in [-2\pi, 0]$, $y \in [-L_y/2, L_y/2]$ and $L_y = 2\pi/k_p$. Figure 12 shows the key properties of the wake. In the linear theory of LWFA ($a_0 \ll 1$), Esarey *et al.* (2009) summarise the following scalings: $E_x \sim E_y \propto a_0^2$ and $B_z \propto a_0^4$

https://doi.org/10.1017/S0022377826101858 Published online by Cambridge University Press

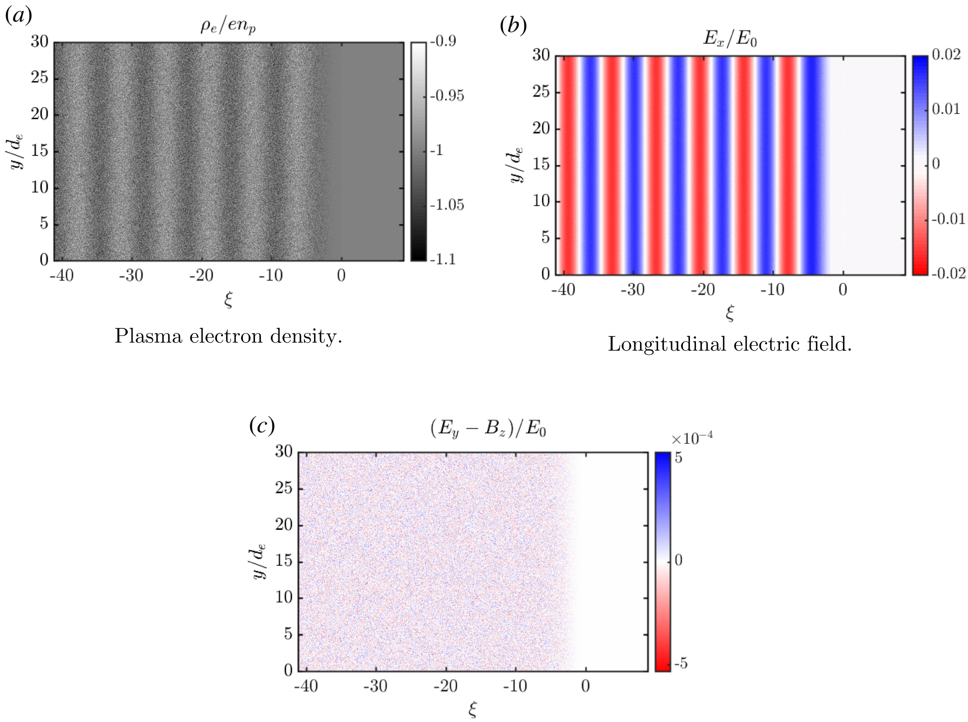

Plasma electron density.

Longitudinal electric field.

Transverse focusing field on a relativistic charge.

FIGURE 11. Two-dimensional simulation of Compton wakefield linear regime ($\mathcal{E}_0 = 0.01\ eE_0/\sigma_T$) with driver transverse size $L_y \gg \lambda_p$.

and one could expect $E_x \sim E_y \propto \mathcal{E}_0$ and $B_z \propto \mathcal{E}_0^2$. The longitudinal electric field retains the one-dimensional form within the driver envelope, approximately, $E_x \simeq (\sigma_T \mathcal{E}_0/e) \sin(\xi) \cos^2(\pi y/L_y)$. Although E_y can be estimated by the transverse derivative of E_x, i.e. $E_y \simeq k_p^{-1} \int d_\xi \partial_y E_x$, the magnetic field exhibits a distinct structure. Part of the longitudinal current produced when photons scatter off fresh plasma is redirected transversely owing to the stochastic character of the Compton force, producing a DC current component resembling the return currents on either side of the driver. The AC part of the current obeys $\partial_\xi E_x \simeq 4\pi J_{AC}/\omega_p$, and the DC part $\langle J_x \rangle_x = J_{DC} = \partial_y B_z/(4\pi c)$. Consequently, B_z is bipolar with a magnitude comparable to E_y, which explains the observed B_z morphology. The DC contribution of B_z produces an offset such that $\langle E_y - B_z \rangle_x \neq 0$. For wider beams, the average DC current vanishes, and the imbalance is not observed.

5.2. *Two-dimensional nonlinear regime*

As stated earlier in the article, nonlinear wakes are excited when $\mathcal{E}_0 \sim eE_0/\sigma_T$. Using the same parameter set as before, we excited a nonlinear wake with a finite-width photon driver shown in figure 13. We have added a fourth subfigure that illustrates the DC current, which is more pronounced in the presence of nonlinear wakes. The previously proposed explanation for the emergence of a DC magnetic component remains valid, and the net transverse field acting on a relativistic electron is therefore always focusing. The characteristic bubble morphology familiar from

https://doi.org/10.1017/S0022377826101858 Published online by Cambridge University Press

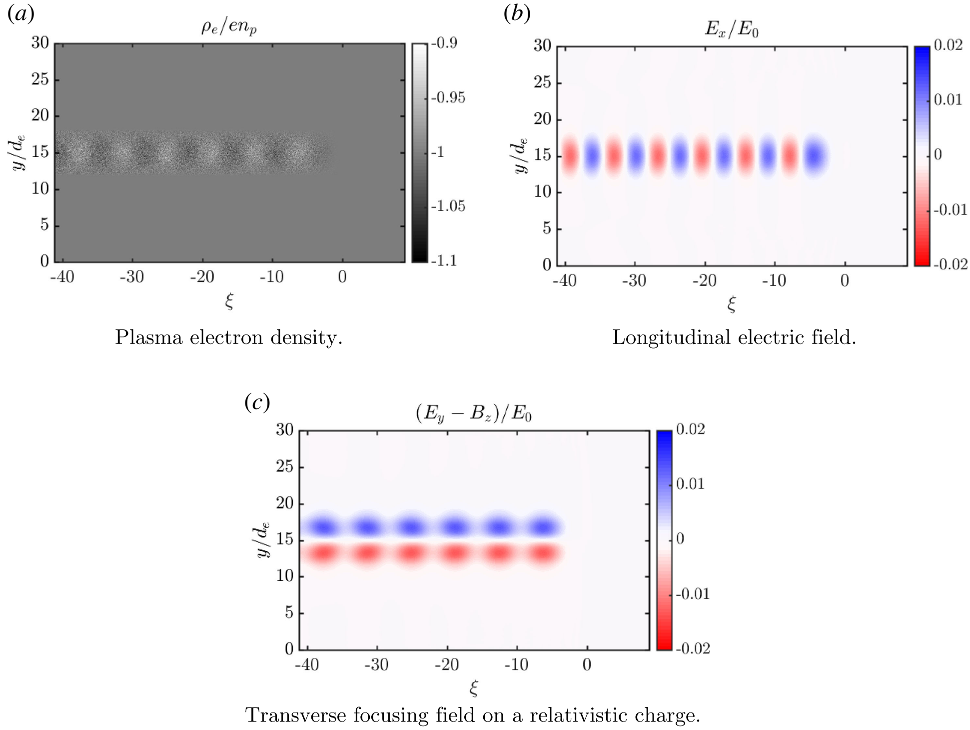

Plasma electron density.

Longitudinal electric field.

Transverse focusing field on a relativistic charge.

FIGURE 12. Two-dimensional simulation of Compton wakefield linear regime ($\mathcal{E}_0 = 0.01\, eE_0/\sigma_T$) with driver transverse size $L_y \simeq \lambda_p$.

LWFA is only partially reproduced. Because the Compton driving force acts predominantly along the longitudinal coordinate ξ, whereas a laser ponderomotive force displaces the electron fluid comparably in longitudinal and transverse directions, the resulting electron cavity is more elongated.

6. Discussion and conclusions

6.1. *Summary*

In this work, we have explored the generation of plasma wakes by non-ponderomotive drivers, specifically photon bursts where the dominant interaction is Compton scattering. This regime is realised when the photon wavelength is much smaller than the interparticle distance but still exceeds the Compton wavelength λ_C. When $\lambda < \lambda_C$, the momentum transfer becomes significant, allowing the electrons to be driven to relativistic velocities and effectively stream with the photons. We reviewed the linear theory for photon-burst-driven wakes and extended it to non-symmetric drivers. Our findings indicate that plasma waves can attain amplitudes comparable to those driven resonantly, with $E \sim \sigma_T \mathcal{E}/e$, provided the photon burst's onset and decay occur over lengths of the order of the resonant length. As detailed in our prior work (Del Gaudio *et al.* 2020*a*), well-defined linear wakes are observable when $\nu_c > \omega_p$. The criteria for nonlinear Langmuir wake formation mirror those established for laser or particle drivers, notably when $\mathcal{E}_0 \gtrsim eE_0/\sigma_T$. Interestingly, even in extreme conditions where $\mathcal{E}_0 \gg eE_0/\sigma_T$, the wake amplitude remains proportional to the energy density, as for the linear theory. Acceleration

https://doi.org/10.1017/S0022377826101858 Published online by Cambridge University Press

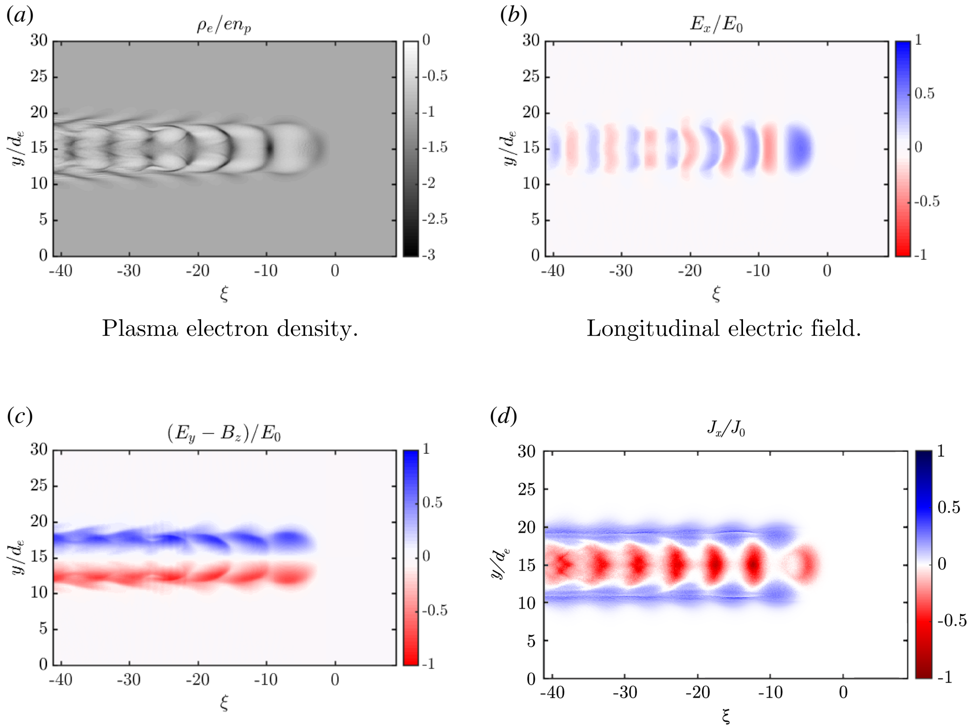

FIGURE 13. Two-dimensional simulation of Compton wakefield nonlinear regime ($\mathcal{E}_0 = eE_0/\sigma_T$) with driver transverse size $L_y \simeq \lambda_p$.

in Compton wakes presents several important characteristics: (i) for a hypothetical perfectly collimated driver,[1] the wake propagates at exactly the speed of light; (ii) electrons can phase-lock within the wake, though the photon driver's depletion length ultimately limits their acceleration; and (iii) non-collimated drivers introduce an effective subluminal phase velocity, with acceleration constrained by the corresponding dephasing length. Our two-dimensional simulations revealed additional nuanced behaviours: although the longitudinal component of the wake aligns well with one-dimensional predictions, the transverse fields differ markedly from those observed in conventional laser wakefields. This discrepancy stems from the plasma response to the driver, which induces a longitudinal current along the axis and results in a DC magnetic field buildup behind the wake. Consequently, the transverse fields are consistently focused at all positions within the wake, highlighting a unique feature of this regime.

6.2. *Compton wakes in the laboratory and in astrophysics*

The possible observation of Compton wakes in the laboratory requires high-frequency photons and a driver with a length of the order of the plasma wavelength. The maximum photon energy density for an X-ray free-electron laser is typically

[1]A perfectly collimated photon driver does not exist in nature. It is a theoretical object to study the limit of Compton wake acceleration.

https://doi.org/10.1017/S0022377826101858 Published online by Cambridge University Press

of the order of $10^{12}\,\mathrm{erg\,cm^{-3}}$. Equation (3.1) reveals that the nonlinear regime could only be accessible for extremely low-density plasmas ($n_p \sim \mathrm{cm^{-3}}$). The plasma would have to be several kilometres long, which makes this nonlinear behaviour out of reach in the laboratory with current technology. As discussed in our previous work, linear Compton wakes may be observed in the future for a plasma density $n_p \sim 10^{17}\,\mathrm{cm^{-3}}$ with a non-resonant driver of length $L/\lambda_p = 10$ (duration of 40 fs), and 100 eV X-rays. The required energy density would be $\mathcal{E} \sim 10^{16}\,\mathrm{erg\,cm^{-3}}$, and the total energy of the driver would be a few joules, which is still orders of magnitude above the energy of an X-ray free-electron laser.

Whereas low-density and very long plasmas are hard to produce in the laboratory, they are naturally present in the interstellar medium. We should therefore determine whether the observed extreme luminosities could potentially correspond to a photon energy density capable of driving nonlinear Compton wakes. Considering a spherical object of radius r_0 and surface $4\pi r_0^2$, the luminosity and the radiation energy density are related by

$$\mathcal{E} = \frac{\mathcal{L}}{4\pi r_0^2 c} \sim 10^{14} \frac{\mathcal{L}[\mathcal{L}_{edd}]}{r_0^2[10^6\mathrm{cm}]} \mathrm{erg\,cm^{-3}}. \tag{6.1}$$

Comparing this expression with (3.1) indicates that radiation from extremely luminous compact objects $\mathcal{L} \gg \mathcal{L}_{edd} \sim 10^{38}\,\mathrm{erg\,s^{-1}}$, propagating into low–density plasmas, can drive the development of nonlinear plasma wakes. The acceleration efficiency follows from the scaling derived in § 4. Equation (4.8) with $E_x \sim E_0$ can be expressed as $\gamma_{\max} \sim (n_p r_e^3)^{-1/2}$, which applied to a plasma of $n_p \sim \mathrm{cm^{-3}}$ yields unphysically large Lorentz factors of 10^{21}. More realistically, the photon burst should have an energy density that decreases during the propagation due to geometric dilution of the photon surface, $\mathcal{E} \sim \mathcal{E}_0 r_0/(r_0 + ct)^2$, which reduces the attainable Lorentz factor to

$$\gamma_{\max} \sim \frac{r_0}{d_e} = r_0[10^6\mathrm{cm}]\sqrt{n_p[\mathrm{cm^{-3}}]}. \tag{6.2}$$

Maximum acceleration efficiency is achieved for resonant drivers, implying that for very tenuous plasmas, the photon-burst duration must be shorter than a few milliseconds.

Acknowledgements

We acknowledge valuable discussions with Dr P. Bilbao and Professor A. Spitkovsky. The authors acknowledge the anonymous referee for pointing out the correct formula for the relativistic Compton force.

Editor Victor Malka thanks the referees for their advice in evaluating this article.

Funding

This work was supported by the European Research Council under grant no. 695088 (ERC-2015-AdG) and by the Portuguese Foundation for Science and Technology (FCT) through grant no. PD/BD/114323/2016 within the framework of the Advanced Program in Plasma Science and Engineering (APPLAuSE, FCT grant no. PD/00505/2012), and the project X-MASER-2022.02230.PTDC. We also acknowledge PRACE and Euro HPC for providing access to the MareNostrum supercomputing resources in Spain. Computational simulations were conducted on the IST cluster in Portugal and the MareNostrum supercomputer in Spain.

Declaration of interests

The authors report no conflict of interest.

REFERENCES

AKHIEZER, A.I. & POLOVIN, R.V. 1956 Theory of wave motion of an electron plasma. *Sov. Phys. JETP* **3**, 696.

BELOBORODOV, A.M. 2023 Monster radiative shocks in the perturbed magnetospheres of neutron stars. *Astrophys. J.* **959**, 34.

BLUMENTHAL, G.R. 1974 The Poynting-Robertson effect and eddington limit for electrons scattering with hard photons. *Astrophys. J.* **188**, 121–130.

CHEN, P., DAWSON, J.M., HUFF, R.W. & KATSOULEAS, T. 1985 Acceleration of electrons by the interaction of a bunched electron beam with a plasma. *Phys. Rev. Lett.* **54**, 693–696.

CHEN, P., TAJIMA, T. & TAKAHASHI, Y. 2002 Plasma wakefield acceleration for ultrahigh-energy cosmic rays. *Phys. Rev. Lett.* **89**, 161101.

CLAYTON, C.E., JOSHI, C., DARROW, C. & UMSTADTER, D. 1985 Relativistic plasma-wave excitation by collinear optical mixing. *Phys. Rev. Lett.* **54**, 2343–2346.

CORDE, S. *et al.* 2015 Multi-gigaelectronvolt acceleration of positrons in a self-loaded plasma wakefield. *Nature* **524**, 442–445.

DAWSON, J.M. 1959 Nonlinear electron oscillations in a cold plasma. *Phys. Rev.* **113**, 383–387.

DEL GAUDIO, F., FONSECA, R.A., SILVA, L.O. & GRISMAYER, T. 2020*a* Plasma wakes driven by photon bursts via compton scattering. *Phys. Rev. Lett.* **125**, 265001.

DEL GAUDIO, F., GRISMAYER, T., FONSECA, R.A. & SILVA, L.O. 2020*b* Compton scattering in particle-in-cell codes. *J. Plasma Phys.* **86**, 905860516.

ESAREY, E. & PILLOFF, M. 1995 Trapping and acceleration in nonlinear plasma waves. *Phys. Plasmas* **2**, 1432–1436.

ESAREY, E., SCHROEDER, C.B. & LEEMANS, W.P. 2009 Physics of laser-driven plasma-based electron accelerators. *Rev. Mod. Phys.* **81**, 1229–1285.

ESAREY, E., SPRANGLE, P., KRALL, J. & TING, A. 1996 Overview of plasma-based accelerator concepts. *IEEE Trans. Plasma Sci.* **24**, 252–288.

FAURE, J., GLINEC, Y., PUKHOV, A., KISELEV, S., GORDIENKO, S., LEFEBVRE, E., ROUSSEAU, J.-P., BURGY, F. & MALKA, V. 2004 A laser–plasma accelerator producing monoenergetic electron beams. *Nature* **431**, 541–544.

FAURE, J.C., TORDEUX, D., GREMILLET, L. & LEMOINE, M. 2024 High-energy acceleration phenomena in extreme-radiation–plasma interactions. *Phys. Rev. E* **109**, 015203.

FONSECA, R.A. *et al.* 2002 Osiris: A three-dimensional, fully relativistic particle in cell code for modeling plasma based accelerators. In *Computational Science — ICCS 2002* (ed. Peter M.A. Sloot, Alfons G. Hoekstra, C.J. Kenneth Tan & Jack J. Dongarra), pp. 342–351. Springer.

GEDDES, C.G.R., TOTH, C., VAN TILBORG, J., ESAREY, E., SCHROEDER, C.B., BRUHWILER, D., NIETER, C., CARY, J. & LEEMANS, W.P. 2004 High-quality electron beams from a laser wakefield accelerator using plasma-channel guiding. *Nature* **431**, 538–541.

HENRI, G. & PELLETIER, G. 1991 Relativistic electron-positron beam formation in the framework of the two-flow model for active galactic nuclei. *Astrophys. J. Lett.* **383**, L7.

HOSHINO, M. 2008 Wakefield acceleration by radiation pressure in relativistic shock waves. *Astrophys. J.* **672**, 940–956.

KURAMITSU, Y., SAKAWA, Y., KATO, T., TAKABE, H. & HOSHINO, M. 2008 Nonthermal acceleration of charged particles due to an incoherent wakefield induced by a large-amplitude light pulse. *Astrophys. J.* **682**, L113–L116.

LANDAU, L.D. & LIFSHITZ, E.M. 1975 *The Classical Theory of Fields*. Pergamon Press.

LANDAU, L.D. & LIFSHITZ, E.M. 1982 *Quantum Electrodynamics*. Pergamon Press.

LI, Z.-Y., BEGELMAN, M.C. & CHIUEH, T. 1992 The effects of radiation drag on radial, relativistic hydromagnetic winds. *Astrophys. J.* **384**, 567.

LU, W., HUANG, C., ZHOU, M., MORI, W.B. & KATSOULEAS, T. 2006 Nonlinear theory for relativistic plasma wakefields in the blowout regime. *Phys. Rev. Lett.* **96**, 165002.

LU, W., TZOUFRAS, M., JOSHI, C., TSUNG, F.S., MORI, W.B., VIEIRA, J., FONSECA, R.A. & SILVA, L.O. 2007 Generating multi-gev electron bunches using single stage laser wakefield acceleration in a 3d nonlinear regime. *Phys. Rev. ST Accel. Beams* **10**, 061301.

MADAU, P. & THOMPSON, C. 2000 Relativistic winds from compact gamma-ray sources. I. radiative acceleration in the Klein-Nishina regime. *Astrophys. J.* **534**, 239.

MANGLES, S.P.D. *et al.* 2004 Monoenergetic beams of relativistic electrons from intense laser–plasma interactions. *Nature* **431**, 535–538.

MARTINEZ, B., GRISMAYER, T. & SILVA, L.ÍS O. 2021 Compton-driven beam formation and magnetization via plasma microinstabilities. *J. Plasma Phys.* **87**, 905870313.

ODELL, S.L. 1981 Radiation force on a relativistic plasma and the eddington limit. *Astrophys. J.* **243**, L147–L149.

PANOFSKY, W.K.H. & WENZEL, W.A. 1956 Some considerations concerning the transverse deflection of charged particles in radio-frequency fields. *Rev. Sci. Instrum.* **27**, 967–967.

PETROFF, E., HESSELS, J.W.T. & LORIMER, D.R. 2019 Fast radio bursts. *Astron. Astrophys. Rev.* **27**, 4.

PEYRAUD, J. 1968 Théorie cinétique des plasmas, interaction matière-rayonnement. I. Action d'un rayonnement donné sur la fonction de distribution électronique par l'intermédiaire des chocs Compton. *J. Phys-PARIS.* **29**, 88–96.

PHINNEY, E.S. 1982 Acceleration of a relativistic plasma by radiation pressure. *Mon. Not. R. Astron. Soc.* **198**, 1109–1118.

PUKHOV, A. & MEYER-TER VEHN, J. 2002 Laser wake field acceleration: the highly non-linear broken-wave regime. *Appl. Phys. B* **74**, 355–361.

SHADWICK, B.A., SCHROEDER, C.B. & ESAREY, E. 2009 Nonlinear laser energy depletion in laser-plasma accelerators. *Phys. Plasmas* **16**, 056704.

SHUKLA, P.K., STENFLO, L., BINGHAM, R., BETHE, H.A., DAWSON, J.M. & MENDONÇA, J.T. 1998 The neutrino electron accelerator. *Phys. Plasmas* **5**, 1–3.

SILVA, L.O., BINGHAM, R., DAWSON, J.M., MENDONÇA, J.T. & SHUKLA, P.K. 1999 Neutrino driven streaming instabilities in a dense plasma. *Phys. Rev. Lett.* **83**, 2703–2706.

SPRANGLE, P., ESAREY, E. & TING, A. 1990 Nonlinear theory of intense laser-plasma interactions. *Phys. Rev. Lett.* **64**, 2011–2014.

SVEDUNG WETTERVIK, B., GONOSKOV, A. & MARKLUND, M. 2018 Prospects and limitations of wakefield acceleration in solids. *Phys. Plasmas* **25**, 013107.

TAJIMA, T. & DAWSON, J.M. 1979 Laser electron accelerator. *Phys. Rev. Lett.* **43**, 267–270.

ZHANG, X., TAJIMA, T., FARINELLA, D., SHIN, Y., MOUROU, G., WHEELER, J., TABOREK, P., CHEN, P., DOLLAR, F. & SHEN, B. 2016 Particle-in-cell simulation of x-ray wakefield acceleration and betatron radiation in nanotubes. *Phys. Rev. Accel. Beams* **19**, 101004.